

Observations of ELF Fields Near the Low-Altitude CRRES Chemical Releases

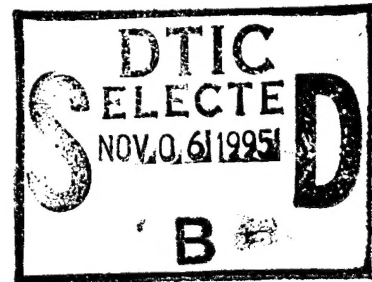
1 August 1995

Prepared by

H. C. KOONS and J. L. ROEDER
Space and Environment Technology Center
Technology Operations

Prepared for

SPACE AND MISSILE SYSTEMS CENTER
AIR FORCE MATERIEL COMMAND
2430 E. El Segundo Boulevard
Los Angeles Air Force Base, CA 90245



Engineering and Technology Group

APPROVED FOR PUBLIC RELEASE;
DISTRIBUTION UNLIMITED

ALL INFORMATION CONTAINED
HEREIN IS UNCLASSIFIED
DATE 11/11/94 BY 10400/100



THE AEROSPACE
CORPORATION
El Segundo, California

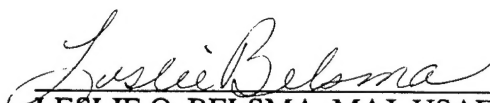
DTIC QUALITY INSPECTED

19951103 014

This report was submitted by The Aerospace Corporation, El Segundo, CA 90245-4691, under Contract No. F04701-93-C-0094 with the Space and Missile Systems Center, 2430 E. El Segundo Blvd., Suite 6037, Los Angeles AFB, CA 90245-4687. It was reviewed and approved for The Aerospace Corporation by A. B. Christensen, Principal Director, Space and Environment Technology Center. Major Leslie O. Belsma was the project officer for the Mission-Oriented Investigation and Experimentation (MOIE) program.

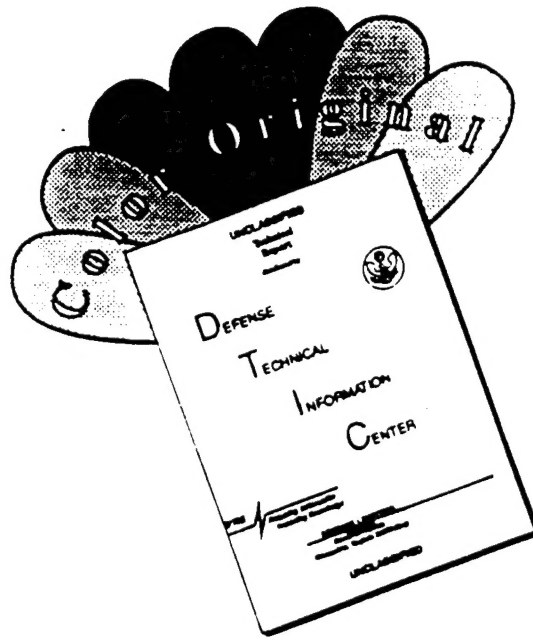
This report has been reviewed by the Public Affairs Office (PAS) and is releasable to the National Technical Information Service (NTIS). At NTIS, it will be available to the general public, including foreign nationals.

This technical report has been reviewed and is approved for publication. Publication of this report does not constitute Air Force approval of the report's findings or conclusions. It is published only for the exchange and stimulation of ideas.


LESLIE O. BELSMA, MAJ, USAF
MOIE Project Officer

Aerospace Corp	
NTIS GRA&I	<input type="checkbox"/>
DTIC TAB	<input type="checkbox"/>
Unannounced	<input type="checkbox"/>
Justification	
By	
Distribution/	
Availability Codes	
Avail	Avail and/or
Spec	Spec

DISCLAIMER NOTICE



THIS DOCUMENT IS BEST QUALITY AVAILABLE. THE COPY FURNISHED TO DTIC CONTAINED A SIGNIFICANT NUMBER OF COLOR PAGES WHICH DO NOT REPRODUCE LEGIBLY ON BLACK AND WHITE MICROFICHE.

REPORT DOCUMENTATION PAGE			Form Approved OMB No. 0704-0188	
Public reporting burden for this collection of information is estimated to average 1 hour per response, including the time for reviewing instructions, searching existing data sources, gathering and maintaining the data needed, and completing and reviewing the collection of information. Send comments regarding this burden estimate or any other aspect of this collection of information, including suggestions for reducing this burden to Washington Headquarters Services, Directorate for Information Operations and Reports, 1215 Jefferson Davis Highway, Suite 1204, Arlington, VA 22202-4302, and to the Office of Management and Budget, Paperwork Reduction Project (0704-0188), Washington, DC 20503.				
1. AGENCY USE ONLY (Leave blank)		2. REPORT DATE 1 August 1995		3. REPORT TYPE AND DATES COVERED
4. TITLE AND SUBTITLE Observations of ELF Fields Near the Low-Altitude CRRES Chemical Releases			5. FUNDING NUMBERS F04701-93-C-0094	
6. AUTHOR(S) Koons, Harry C.; and Roeder, James L.				
7. PERFORMING ORGANIZATION NAME(S) AND ADDRESS(ES) The Aerospace Corporation Technology Operations El Segundo, CA 90245-4691			8. PERFORMING ORGANIZATION REPORT NUMBER TR-94(4940)-10	
9. SPONSORING/MONITORING AGENCY NAME(S) AND ADDRESS(ES) Space and Missile Systems Center Air Force Materiel Command 2430 E. El Segundo Blvd. Los Angeles Air Force Base, CA 90245			10. SPONSORING/MONITORING AGENCY REPORT NUMBER SMC-TR-95-35	
11. SUPPLEMENTARY NOTES				
12a. DISTRIBUTION/AVAILABILITY STATEMENT Approved for public release; distribution unlimited			12b. DISTRIBUTION CODE	
13. ABSTRACT (Maximum 200 words) The Combined Release and Radiation Effects Satellite (CRRES) performed a series of seven low-altitude chemical releases between September 10, 1990, and August 12, 1991. Immediately following each chemical release, electric and magnetic fields were detected by the extremely low frequency wave analyzer sensors of the Low Altitude Satellite Studies of Ionospheric Irregularities (LASSII) experiment on the spacecraft. The time series and spectra of the two field components are quite similar for each of the releases but vary in detail from release to release. The index of refraction estimated from the ratio of the magnetic field to the electric field is too small by about 2 orders of magnitude for either the right-hand wave or the extraordinary wave modes which are the only propagating electromagnetic modes in the detected band above the O ⁺ ion gyrofrequency (~30 Hz). ELF hiss observed at higher altitudes is found to be propagating in the extraordinary wave mode with the correct index of refraction. This confirms that the intensity measurements are being made correctly by the instrument and that an alternative explanation is required for the signals detected following the chemical releases. We show that the waves are primarily electrostatic and that the magnitude of the wave magnetic field is consistent with the transverse magnetic field component of ion acoustic waves.				
14. SUBJECT TERMS Chemical release Ionosphere Electrostatic waves			15. NUMBER OF PAGES 13	
			16. PRICE CODE	
17. SECURITY CLASSIFICATION OF REPORT Unclassified	18. SECURITY CLASSIFICATION OF THIS PAGE Unclassified	19. SECURITY CLASSIFICATION OF ABSTRACT Unclassified	20. LIMITATION OF ABSTRACT	

Observations of ELF fields near the low-altitude CRRES chemical releases

H. C. Koons and J. L. Roeder

Space and Environment Technology Center, The Aerospace Corporation, Los Angeles, California

Abstract. The Combined Release and Radiation Effects Satellite (CRRES) performed a series of seven low-altitude chemical releases between September 10, 1990, and August 12, 1991. Immediately following each chemical release, electric and magnetic fields were detected by the extremely low frequency wave analyzer sensors of the Low Altitude Satellite Studies of Ionospheric Irregularities (LASSII) experiment on the spacecraft. The time series and spectra of the two field components are quite similar for each of the releases but vary in detail from release to release. The index of refraction estimated from the ratio of the magnetic field to the electric field is too small by about 2 orders of magnitude for either the right-hand wave or the extraordinary wave modes which are the only propagating electromagnetic modes in the detected band above the O^+ ion gyrofrequency (~ 30 Hz). ELF hiss observed at higher altitudes is found to be propagating in the extraordinary wave mode with the correct index of refraction. This confirms that the intensity measurements are being made correctly by the instrument and that an alternative explanation is required for the signals detected following the chemical releases. We show that the waves are primarily electrostatic and that the magnitude of the wave magnetic field is consistent with the transverse magnetic field component of ion acoustic waves.

Introduction

The Combined Release and Radiation Effects Satellite (CRRES) performed a series of seven low-altitude chemical releases between September 10, 1990, and August 12, 1991. The chemical release mission is described by Reasoner [1992]. Two releases below the terminator at dusk in the vicinity of American Samoa in the South Pacific tested theories for critical velocity ionization, a process which may produce a large amount of ionization as a neutral gas moves at high speed across the magnetic field in the ionosphere. Other releases took place in sunlight at dawn in the Caribbean. The objectives include studying the flow of the ions from the Caribbean to the conjugate point in the southern hemisphere and the studying of the response of the ionosphere to selected perturbations. Small and large canisters of barium and large canisters of strontium and calcium were released. Table 1 contains a list of the parameters for the seven releases.

Immediately following each chemical release, electric and magnetic fields were detected by the extremely low frequency wave analyzer (ELFWA) sensors of the Low Altitude Satellite Studies of Ionospheric Irregularities (LASSII) experiment on the spacecraft. The time series and spectra of the two field components are quite similar for each of the releases but vary in detail from release to release. The measurements reported here are the first measurements of extremely low frequency (ELF) magnetic fields excited by chemical releases in the ionosphere that have been made with a high-sensitivity (0.2 pT) receiver specifically designed to measure the magnetic field component of electromagnetic

waves at ELF. Previous measurements of emissions have been made with only electric field sensors [Kelley *et al.*, 1974; Koons and Pongratz, 1979; Holmgren *et al.*, 1980; Kelley *et al.*, 1986; Brenning *et al.*, 1991] or with electric field sensors and a low-sensitivity aspect magnetometer for the magnetic field sensors [Whalen *et al.*, 1985; Swenson *et al.*, 1990; Kelley *et al.*, 1991; Bolin and Brenning, 1993].

The aspect magnetometers typically measure ultralow-frequency magnetic perturbations caused by macroscopic currents flowing along the magnetic field line. For example, Bolin and Brenning [1993] describe the field observations during the CRIT II barium release as turbulent electric fields from electrostatic instabilities with lower frequency and more coherent oscillations in the magnetic field near the barium ion gyrofrequency. Also, using the magnetic field measurements during this same experiment, Swenson *et al.* [1990] calculate that a field-aligned current of 11 mA/m² is consistent with the observed ≈ 300 nT low-frequency magnetic perturbations during the first few tenths of a second after the barium release.

In this paper we describe the ELF electric and magnetic fields from the low-altitude CRRES chemical releases detected by the ELFWA sensors on the CRRES spacecraft.

Instrument Description

The ELFWA measures single-axis electric field spectra and amplitudes from 2 to 250 Hz and single-axis magnetic field spectra and amplitudes from 2 to 125 Hz. Two antennas, two preamplifiers, and two electronics boxes comprise the instrument. The electric field sensor consists of two spherical probes each 6.35 cm in diameter on booms 190.5 cm long deployed above the spacecraft. The probes are 4.5 m apart. The signals from the two probes are differenced in the *E* field electronics package to provide a single-axis

Table 1. CRRES Low-Altitude Chemical Releases

Release	Date	Time UT, hmin:s	Latitude, deg	Longitude, deg	Altitude, km	Chemicals, kg
G-13	Sept. 10, 1990	0610:25	17.5 S	198.9 E	517	5.4 Ba 3.8 Sr
G-14	Sept. 14, 1990	0847:10	18.1 S	161.6 E	593	5.4 Ba 1.9 Ca
G-01	July 13, 1991	0835:25	17.8 N	62.9 W	495	1.5 Ba
G-09	July 19, 1991	0837:07	17.4 N	62.8 W	441	10.8 Ba
G-11a	July 22, 1991	0838:24	16.8 N	60.3 W	411	1.5 Ba
G-11b	July 25, 1991	0837:11	17.3 N	69.5 W	478	1.5 Ba
G-12	Aug. 12, 1991	0931:20	9.1 N	63.5 W	507	3.0 Ba

electric field measurement which rotates in the spin plane of the spacecraft.

The magnetic field antenna is a 50-cm-diameter, 1600-turn loop deployed on a 2-m boom. The frequency response of the *B* field antenna is 6 dB per octave in the 12.5–125 Hz frequency range. The preamplifier has been frequency compensated with 6 dB per octave bass boost to produce a flat frequency response from the antenna and preamplifier combination from 10–125 Hz. The single-axis magnetic field component rotates in the spin plane of the spacecraft. However, it is not parallel to the electric field component measured by the electric antenna.

The *E* field and *B* field signals are sampled at evenly spaced intervals at 250 samples per second providing a 125-Hz Nyquist frequency for the signal from each antenna. Each of the electronics packages has independent gain settings of 0, –20, and –40 dB and two modes, linear and automatic gain control (AGC). The dynamic range is 48 dB in the linear mode and approximately 90 dB in the AGC mode at one gain setting. The decay time constant of the AGC circuit is approximately 2 s, and the AGC voltage is monitored once every 2 s. For the chemical releases the experiment took data in the AGC mode with the gain set at 0 dB. The sensitivity corresponding to 0.02 V (1 bit) output from the electronics packages is 9.9×10^{-7} V/m from the electric antenna and 0.2 pT from the magnetic antenna. The broadband signal (i.e., the total signal in-band from 2 to 125 Hz) is also averaged and recorded each second. A more complete description of the instrument is given by Koons *et al.* [1992].

Broadband Data

The broadband signals from the seven chemical releases are qualitatively quite similar. The large barium release on July 19, 1991, will be used to describe the data. Figure 1 shows the broadband signal within the band of the receivers during a perigee data acquisition on July 19, 1991. The top panel shows the electric field, and the bottom panel shows the magnetic field. The large spike in both channels at 0837:07 UT resulted from the G-09 chemical release. The cause of the background signal in the magnetic channel around that time is not known. It may be electromagnetic interference (EMI) or it may be the magnetic component of an electromagnetic wave propagating in a mode for which the electric field component is below the noise level of the broadband measurement. The signals after 0848 UT are

caused by ELF hiss propagating in the extraordinary mode. They will be discussed briefly below.

Plate 1 shows the spectrogram of the fields about the time of the G-09 chemical release. The horizontal lines in Plate 1 are EMI. The vertical band immediately following 0837:01 UT is the signature of this chemical release. The spectrum is almost unstructured. Near the beginning of the signal associated with the chemical release the lowest frequencies are somewhat stronger than they are near the end of the signal.

Figure 2 shows an expanded view of the broadband signal for a 50-s period about the time of the release together with plots of the angle between the sensed component and the Earth's magnetic field. Each sample represents a 1-s average of the signal. The antenna angles are not in phase with each other because the sense directions of the two antennas are not parallel. This release, consisting of two large barium canisters in sunlight, was the largest. The signal increases abruptly at 0837:07, the nominal time of the release. The signals in each component last less than 15 s. The magnetic component decreases somewhat more rapidly than the electric component. However, the similarity of the shapes of the electric and the magnetic signatures suggest that the decrease represents an approximately exponential decay in time that is unrelated to the antenna sense direction.

Because the signals are present for a time which is significantly shorter than the 30-s spin period of the satellite it is difficult to use the spin to establish the direction of the sensed component with respect to the Earth's magnetic field. Figure 2 does show that both the electric and the magnetic

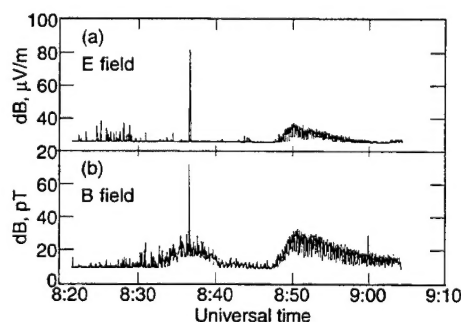


Figure 1. Broadband field intensities versus universal time for the data acquisition containing the G-09 chemical release on July 19, 1991: (a) electric field; (b) magnetic field.

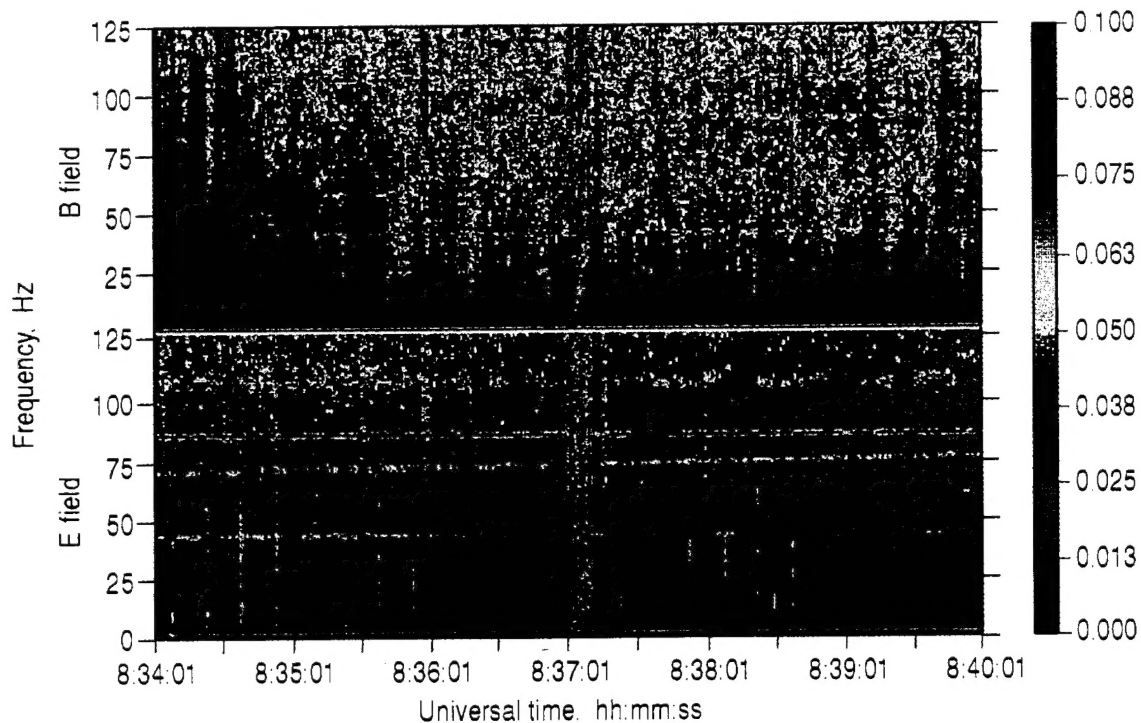


Plate 1. Spectrogram of the field intensities for the G-09 chemical release on July 19, 1991. (top) Magnetic field; (bottom) electric field. The intensity scale is linear but uncalibrated.

signals have significant components parallel to the geomagnetic field and that neither component shows any feature as the antenna sense direction goes through the minimum angle with respect to the geomagnetic field. Similar phasing with-

out any features at the minimum angle with respect to the geomagnetic field for either component also occurred for release G-12. On the other hand, G-13 shows a well-defined minimum in the broadband magnetic field intensity when the magnetic component being sensed is nearly parallel to the geomagnetic field. The signatures of the other four releases were too short to determine any information about the direction of the field components.

Table 2 shows the maximum broadband field intensities measured by the electric and magnetic sensors for each of the seven releases. The values are plotted in Figure 3 as a function of the mass of the barium released. Open circles are used for the releases which took place in sunlight above the terminator, and solid circles are used for the releases that took place in shadow below the terminator (the critical velocity experiments). The intensity of both field components tends to increase with the mass of barium present in the release. For a given mass of barium the releases above

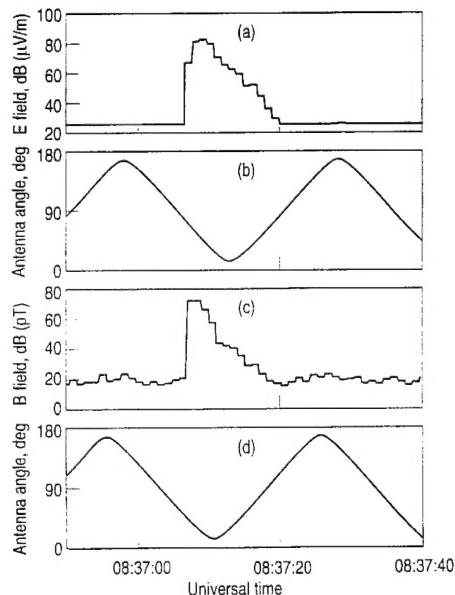


Figure 2. (a) Electric field intensity, (b) electric field antenna angle. (c) magnetic field intensity, and (d) magnetic field antenna angle with respect to the geomagnetic field versus universal time for the G-09 chemical release on July 19, 1991.

Table 2. Maximum Wave Intensities From the Broadband Data for the CRRES Low-Altitude Chemical Releases

Release	Date	E_{\max} , dB(V/m)	B_{\max} , dB(pT)	cB_{\max}/E_{\max}
G-13	Sept. 10, 1990	-52.5	47.0	28
G-14	Sept. 14, 1990	-55.3	47.9	43
G-01	July 13, 1991	-46.2	50.6	21
G-09	July 19, 1991	-38.0	72.0	95
G-11a	July 22, 1991	-55.3	67.8	429
G-11b	July 25, 1991	-61.1	38.4	28
G-12	Aug. 12, 1991	-41.7	60.0	36

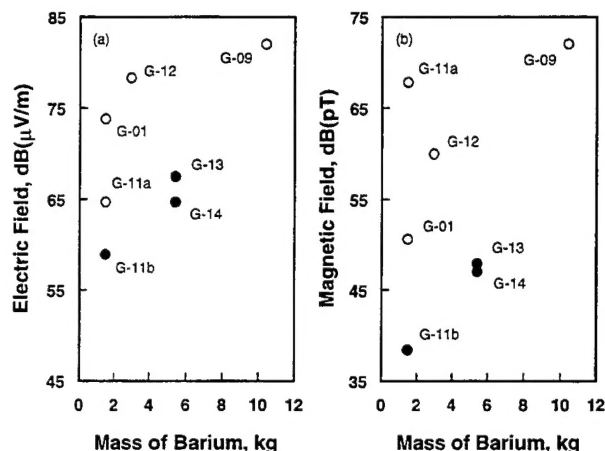


Figure 3. (a) Maximum electric field intensity and (b) maximum magnetic field intensity versus mass of barium contained in the chemical release for the seven low-altitude CRRES chemical releases. Open circles are releases above the terminator, and solid circles are releases below the terminator.

the terminator produced a larger signal than the releases below the terminator. However, the difference between the sunlit and the shadow releases for a comparable mass of barium is only 10 dB. The magnetic field intensity from release G-11a seems to be anomalously high when compared with the other releases. The ratio of cB_{\max}/E_{\max} , where the subscript max refers to the maximum value of the broadband field intensity, is an estimate of the index of refraction of the medium for the dominant electromagnetic wave mode. This quantity is listed for each release in Table 2. Because the antennas are rotating, the electric and magnetic field maxima cannot be rigorously compared. Generally, however, the maxima are temporal rather than spatial and tend to peak within 1 s of each other.

Figure 4 shows the index of refraction for electromagnetic waves at the point of release G-13 computed using the electron density measured by the LASSII Pulsed Plasma Probe experiment [Baumbach *et al.*, 1992]. At the release point the left-hand mode does not propagate between the oxygen ion gyrofrequency at 29 Hz and the upper frequency limit of our measurement at 125 Hz. The index of refraction for the right-hand mode n_r , and the extraordinary mode n_x for releases G-13 and G-09 are shown in Table 3 for a frequency of 40 Hz. The measured values of cB_{\max}/E_{\max} of 28 and 95, respectively, are much less than the calculated values for the index of refraction of the right-hand mode n_r , or of the extraordinary mode n_x as shown in Table 3.

Narrowband Data

A fast Fourier transform routine was used to compute power spectral density estimates of the voltage wave forms measured by each sensor. Spectra were determined from 1 s measurements (250 samples per second) of data for each field component which were taken every second from 2 s before the nominal time of a release to 8 s after.

We have analyzed the first signals detected from each release and compared them with the characteristics of the broadband data and with signals which were detected two to

three seconds after the first arrivals. The later signals are representative of the preponderance of the signals detected.

Early Time Fields

Figure 5 shows the field data in the left panels and the spectra in the right panels for the early time fields from release G-13. The amplitudes of the electric and magnetic fields in Figure 5 as well as in Figures 6–9 are plotted on uncalibrated scales (the telemetered voltage in the range ± 2.5 V), because changes in the AGC in response to the rapidly changing signals preclude precise calibration of the data. The spectra in this set of figures reasonably represent the power spectra of the wave fields. However, they deviate from the true power spectra because of the AGC response of the receiver and because of the slight saturation of the receiver during some of the time periods shown. Saturation is especially evident in the first second or two after a release. The relative error across a spectrum from these effects is no more than a few percent. The G-13 release was performed at low altitudes in the dark for the purpose of testing the critical velocity theory of Alfvén. The spectra of the first arriving waves from releases G-13 and G-14 are quite similar. There is a general increase in power with increasing frequency. The time series and spiky spectra suggest the presence of rather turbulent fields during the first second following these releases. This is a characteristic of each of the seven CRRES releases and has been noted in the electric field measurements from previous chemical releases [Kelley *et al.*, 1986; Swenson *et al.*, 1990; Kelley *et al.*, 1991; Bolin and Brenning, 1993]. The overall similarity of the time series and spectra from both field components suggests that both signals arise from the same source system of currents and charges.

Figure 6 shows the field data in the left panels and the spectra in the right panels from release G-11b. This release was a small barium release that also took place in darkness. The first signals from the release occur near 0.54 s in Figures 6a and 6c. The electric and magnetic field data before a release usually show little structure and have a low amplitude. A typical example is the electric field data in Figure 6 prior to 0.5 s. The magnetic field data in Figure 6 is an

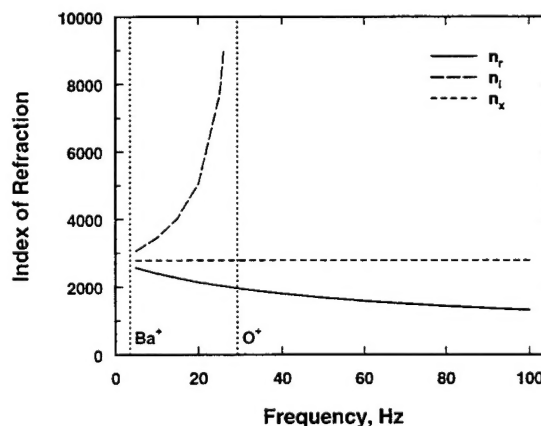


Figure 4. The index of refraction for the right-hand n_r , the left-hand n_l , and the extraordinary n_x , plasma waves as a function of frequency for ionospheric plasma parameters appropriate to chemical release G-13.

Table 3. Examples of the Parameters Used for the Index of Refraction Calculations at a Frequency of 40 Hz for the Chemical Releases and 100 Hz for the ELF Hiss

	Release		
	G-13	G-09	ELF Hiss
Date	Sept. 10, 1990	July 19, 1991	July 19, 1991
Universal time	0610	0837	0851
Altitude, km	517	441	1,728
Electron density, cm^{-3}	2.3×10^6	7.1×10^5	1.1×10^4
Fractional abundance of O^+	1	1	0
Fractional abundance of H^+	0	0	1
Magnetic field, mG	302	316	138
Ion gyrofrequency, Hz	28.8	30.1	210
n_r	1317	960	97
n_l	NA	NA	163
n_x	2786	1465	118
$cB_{\text{max}}/E_{\text{max}}$	28	95	169

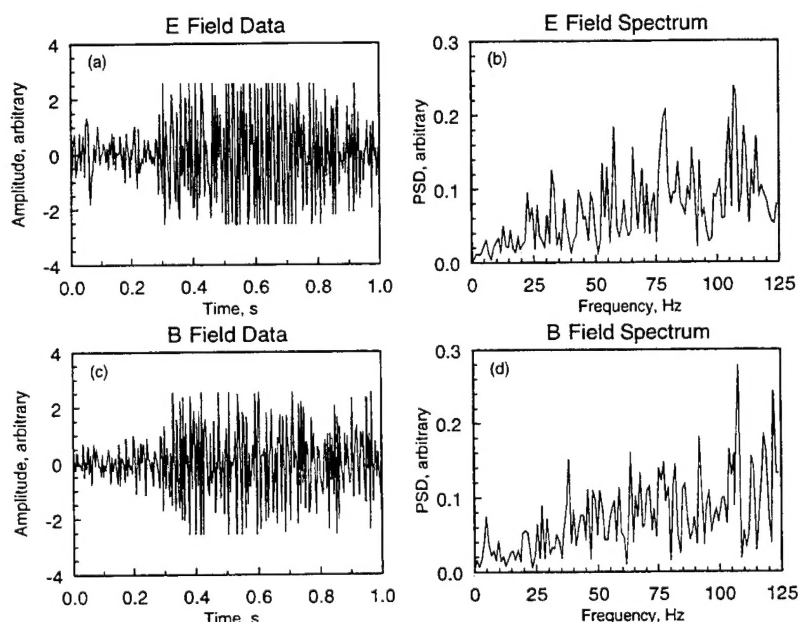
NA, not applicable.

exception. It shows spikes that have induced a larger positive than negative voltage on the antenna. These spikes which show up as lines in the magnetic field spectrum in Figure 6d near 30 and 60 Hz are EMI that was observed well before the release on this particular orbit. Since the oxygen gyrofrequency is 30 Hz, the EMI may be related to a chance coincidence in frequency between a source on the vehicle and the oxygen ion gyrofrequency. The odd one-sided nature of the ac magnetic field signal prior to 0.4 s in Figure 6c is the best indication that these spikes are EMI. The spectra before the release are generally flat, and the total power is negligible compared with the power in the first signals from the release. For example, the electric field power spectrum in Figure 6 is dominated by the signals from the release after 0.5 s.

The similarity of the time series and the spectra again suggest that the fields arise from the same source with frequencies primarily above 80 Hz. No signals are seen near

the barium or the oxygen ion cyclotron frequencies in the electric field data.

Figure 7 shows the field data and spectra from the small barium release, G-11a, which took place in sunlight. It should be compared with G-11b (Figure 6), which was a release of an identical amount of barium in the dark. For G-11a the first signals occurred over the entire frequency range with perhaps a broad peak around 50 Hz and less power above 80 Hz than seen in release G-11b. A comparison of both the time series and the spectra from the two releases clearly shows the lower frequencies in the G-11a spectrum. However, there are no readily discernible features in the spectra that can be associated with the barium (Ω_{Ba^+}) or the oxygen (Ω_{O^+}) ion gyrofrequencies. The absence of a resonance at $\Omega_{\text{O}^+} = 30$ Hz in the magnetic field spectrum indicates that the waves are not propagating in the longitudinal left-hand electromagnetic mode [Gurnett *et al.*, 1965].

**Figure 5.** Time series and spectra of the electric and magnetic fields observed for the G-13 chemical release. Time zero is 0610:24.7 UT on September 10, 1990.

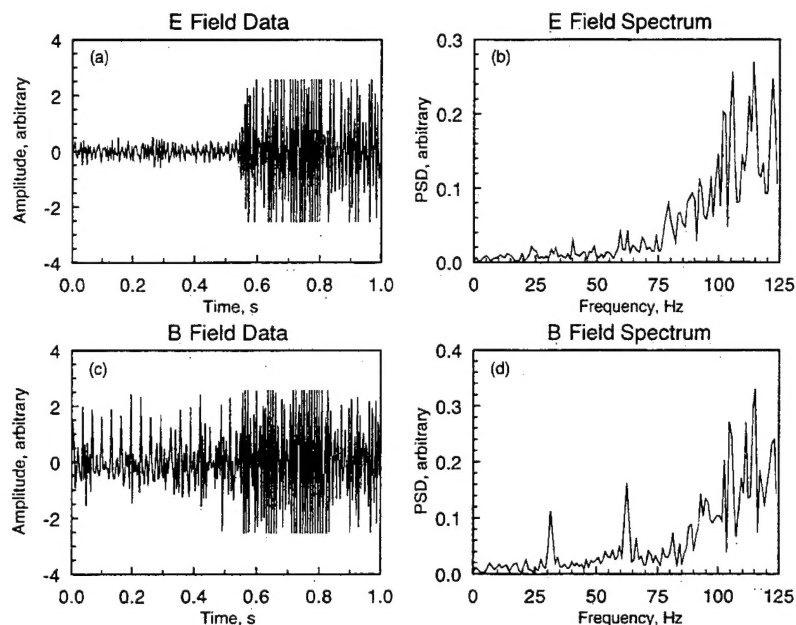


Figure 6. Time series and spectra of the electric and magnetic fields observed for the G-11b chemical release. Time zero is 0837:10.9 UT on July 25, 1991.

Signals from the larger releases in sunlight tended to saturate the receiver for a few seconds after the release. This is especially the case for the two largest releases in sunlight, G-09 and G-12. The spectra indicate that the signals from G-09 were primarily low frequency fields between Ω_{Ba+} and Ω_{O+} .

In summary, the releases in the dark and the small barium releases in sunlight produced little wave excitation near Ω_{Ba+} . The two smaller releases in sunlight, G-01 and G-12,

produced signals near Ω_{O+} , and the largest release in sunlight, G-09, produced large signals near Ω_{Ba+} and Ω_{O+} .

Midevent Fields

The spectra of the fields from each of the releases evolved rapidly after they were first detected at CRRES. A later example from release G-13 is shown in Figure 8. These data were taken 2 s after the data shown in Figure 5. The

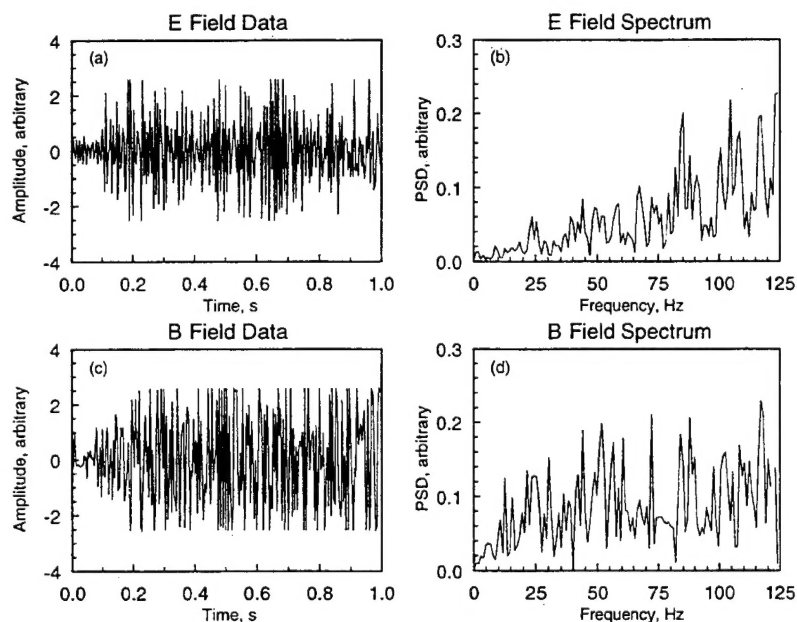


Figure 7. Time series and spectra of the electric and magnetic fields observed for the G-11a chemical release. Time zero is 0838:23.9 UT on July 22, 1991.

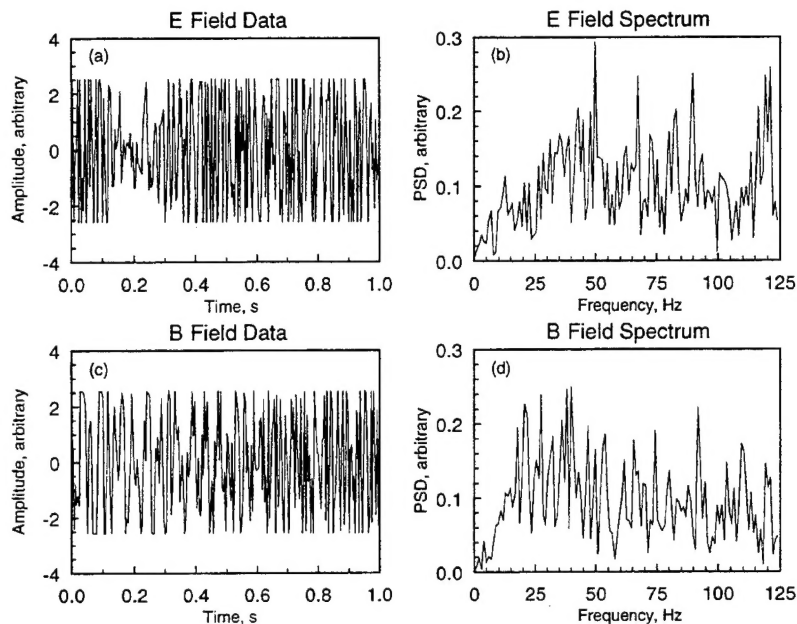


Figure 8. Time series and spectra of the electric and magnetic fields observed for the G-13 chemical release. Time zero is 0610:26.9 UT on September 10, 1990.

amplitude of the fields has increased, and the most intense fields are now occurring at a lower frequency. The overall similarity of the electric and magnetic fields again suggests that the fields are excited by the same source distribution. The lack of any feature associated with the oxygen ion cyclotron frequency also rules out propagation in the left-hand electromagnetic mode.

Figure 9 shows the data from the largest barium release in sunlight, G-09. These data were taken about 3 s after the first

signals were detected at CRRES. They show a spectrum dominated by signals between the barium and the oxygen ion gyrofrequencies. There is also a fairly well defined minimum in both field components at the oxygen ion gyrofrequency 30 Hz.

ELF Hiss

The signals after 0848 UT in Figure 1 are caused by ELF hiss propagating in the extraordinary mode. Figure 10 shows

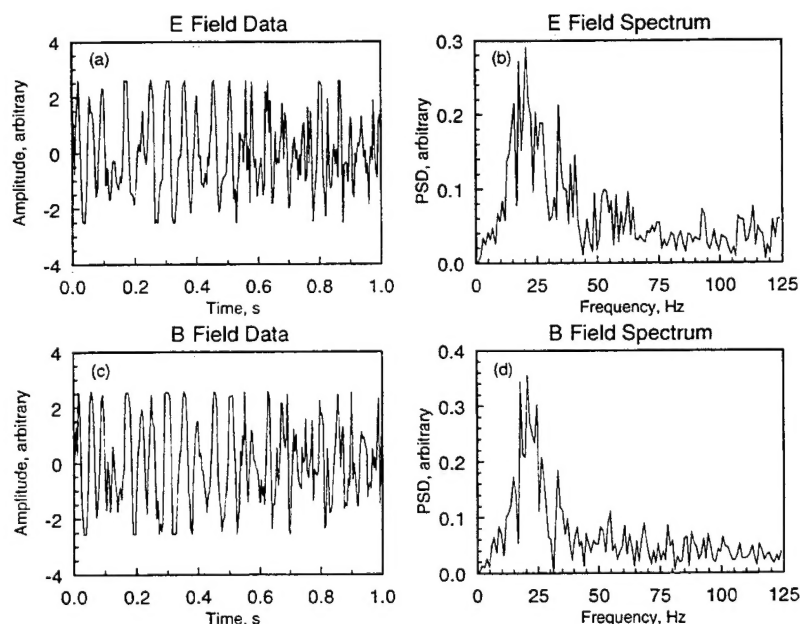


Figure 9. Time series and spectra of the electric and magnetic fields observed for the G-09 chemical release. Time zero is 0837:08.9 UT on July 19, 1991.

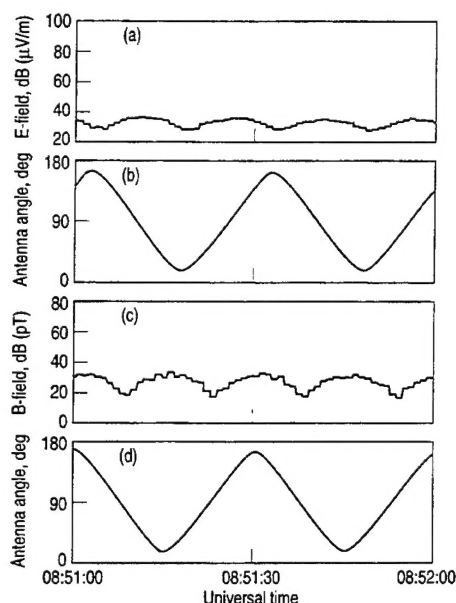


Figure 10. (a) Electric field intensity, (b) electric field antenna angle, (c) magnetic field intensity, and (d) magnetic field antenna angle with respect to the geomagnetic field versus universal time for the ELF hiss observed on July 19, 1991.

expanded views of the broadband signals from the electric and magnetic antennas for a 1-min period at 0851:00 UT during the time when strong ELF hiss was present. In Figure 10 the electric field peaks at an antenna angle of 90° that is perpendicular to the geomagnetic field, and the magnetic field peaks when the antenna angle is a minimum. These angles are consistent with the electromagnetic extraordinary wave in which the wave vector and the electric field vector are perpendicular to the geomagnetic field, and the magnetic field vector is parallel to the geomagnetic field. The computed value for n_x at 100 Hz for this time period from Table 3 is 118, while the measured value of cB_{\max}/E_{\max} is 169. This is reasonable agreement considering that there are several decibels of variation on both the electric and the magnetic field measurements, and we are only measuring the field components in the spin plane of the vehicle.

Discussion

The similarity of the characteristics of the magnetic and electric field signals, both broad band and narrow band, strongly suggests that the signals detected by both sensors following the low-altitude CRRES chemical releases in the detection band of the ELFWA arise from the same source charge and current distributions. However, the measured ratios of cB/E from the broadband data are inconsistent with the index of refraction calculated for the electromagnetic waves that can propagate in this frequency range. The discrepancy is very large, a factor of 50–100. The same is true for the narrow-band data. As an example, for the G-13 release at 0610:27 UT on September 10, 1990, the value of cB/E for the 40 Hz bin is 88. This is only 0.05 n_x and 0.03 n_x .

We suggest that virtually all of the signals detected by the ELFWA in conjunction with the chemical releases arise

from ion plasma waves [Allis *et al.*, 1963]. The magnitude of the wave magnetic field is consistent with that for the magnetic field component of a predominantly electrostatic ion acoustic wave in the frequency band of the ELFWA.

From Maxwell's equations the transverse components E_t and B_t of the wave fields E and B are related to the wave phase velocity u by

$$|E_t|/|B_t| = u = \omega/k \quad (1)$$

where ω is the wave frequency and k is the wave number. The magnetic field of the wave is always transverse to the propagation vector so the measured magnetic field amplitude will be taken as an estimate of $|B_t|$.

At low frequencies, ion plasma waves with propagation vectors along the magnetic field have a phase velocity given by

$$u^2 = \frac{\kappa}{m_+} \left(\gamma_+ T_+ + \frac{\gamma_- T_-}{\gamma_- k^2 \lambda_D^2 + 1} \right) \quad (2)$$

where κ is Boltzmann's constant, m_+ is the ion mass, γ_{\pm} is the specific heat ratio, T_{\pm} is the temperature, k is the wave number, and λ_D is the Debye length. The signs refer to the charge species. For wavelengths that are much longer than the Debye length $k^2 \lambda_D^2 \ll 1$, the phase velocity reduces to the sound speed

$$u_s^2 = \frac{\kappa}{m_+} (\gamma_+ T_+ + \gamma_- T_-) \quad (3)$$

and the waves are known as ion acoustic waves. In the ionosphere, $u_s \approx 10^3$ m/s. From (1) we find that near the center of the ELFWA band at 60 Hz, $k \approx 0.4$ m⁻¹ and $\lambda \approx 16$ m. This is much longer than the Debye length in the ionosphere and several times longer than the length of the ELFWA electric field antenna. Thus the sound speed approximation to the phase velocity is a good one. The antenna pattern will be more complex than the pattern of a simple dipole, but that will not affect the order of magnitude estimates in our calculations.

The transverse component of the electric field that corresponds with the measured value of the magnetic field can be estimated using (1) and the data in Table 2. For the G-13 release the broadband magnetic field is 47 dB(pT) or 2.2×10^{-10} T. For a sound velocity of 10^3 m/s the corresponding electric field is 2.2×10^{-7} V/m. Since the observed electric field was -52 dB(V/m) or 2.5×10^{-3} V/m, the ratio of $|E_t|/|E| \approx 10^{-4}$. Thus the combined field observations are consistent with the fields for predominantly electrostatic ion acoustic waves.

Ion acoustic waves are normally strongly Landau damped. However, chemical releases with high velocity perpendicular to the magnetic field such as the CRRES releases provide a plethora of current systems [Brenning *et al.*, 1991] which may be capable of destabilizing ion acoustic waves. Ion acoustic waves have been observed from a cesium release which did not have a highly directed velocity. In that case, Kintner *et al.* [1980] suggested that the ion acoustic waves were produced by an ion-ion streaming instability between the cesium and the ambient ions.

The spectra of the waves generated by the large G-09 release in sunlight differ from those of the other releases. The first signals from G-09 show peaks at the barium and

oxygen ion gyrofrequencies, and the later signals show attenuation bands at Ω_{O+} . These characteristics are similar to waves identified as ion cyclotron waves from the large Buaro-shaped charge barium release in sunlight [Koons and Pongratz, 1979, 1981]. On the basis of the attenuation bands at the ion gyrofrequencies and the similarity of the waves from the Buaro release the waves from the CRRES G-09 release are identified as ion cyclotron waves.

Conclusions

The ELF electric and magnetic fields detected near each of the seven low-altitude CRRES chemical releases bear a striking similarity for each release but vary in detail from release to release. The spectra show little structure that can be related to characteristic plasma frequencies between 2 and 125 Hz. The amplitudes of the electric and magnetic signals are generally proportional to the mass of the barium in the release with the amplitudes of the signals for the releases in the dark being only 10 dB lower than for the releases in sunlight. Thus the mechanism for the generation of the waves does not require the presence of the prompt ionization from sunlight.

The similarity of the characteristics of the two components strongly suggests that they arise from the same current and charge distributions. Since the wave amplitudes and spectral shapes are inconsistent with electromagnetic modes, we identify the waves as ion acoustic waves which are predominantly electrostatic but also possess small transverse magnetic and electric components. The waves from the largest barium release, G-09, have attenuation bands at the oxygen ion gyrofrequency. These waves are identified as ion cyclotron waves.

Acknowledgments. We wish to express our appreciation to P. Rodriguez, LASSII Principal Investigator, for the opportunity to fly the ELFWA instrument as part of the LASSII experiment. We thank P. Rodriguez and M. Baumbach of NRL for the electron density data from their Pulsed Plasma Probe experiment on LASSII. We also acknowledge the efforts of W. B. Harbridge, S. Imamoto, D. Katsuda, P. Lew, D. Mabry, and W. Wong in the fabrication, testing, and integration of the ELFWA instrument. This work was supported by the Space and Missile Systems Center, Air Force Materiel Command under contract F04701-93-C-94.

The Editor thanks T-Z. Ma and R. R. Anderson for their assistance in evaluating this paper.

References

- Allis, W. P., S. J. Buchsbaum, and A. Bers, *Waves in Anisotropic Plasmas*, MIT Press, Cambridge, Mass., 1963.
- Baumbach, M., P. Rodriguez, D. N. Walker, and C. L. Siefring, LASSII Pulsed Plasma Probe on CRRES, *J. Spacecr. Rockets*, 29, 607-609, 1992.
- Bolin, O., and N. Brenning, Particle simulations of ionospheric injection experiments: Comparison with CRIT II, *J. Geophys. Res.*, 98, 19,081-19,091, 1993.
- Brenning, N., et al., Interpretation of the electric fields measured in an ionospheric critical ionization velocity experiment, *J. Geophys. Res.*, 96, 9719-9733, 1991.
- Gurnett, D. A., S. D. Shawhan, N. M. Brice, and R. L. Smith, Ion cyclotron whistlers, *J. Geophys. Res.*, 70, 1665-1688, 1965.
- Holmgren, G., R. Boström, M. C. Kelley, P. M. Kintner, R. Lundin, U. V. Fahlson, E. A. Bering, and W. R. Sheldon, Trigger, an active release experiment that simulated auroral particle precipitation and wave emissions, *J. Geophys. Res.*, 85, 5043-5053, 1980.
- Kelley, M. C., A. Pedersen, U. V. Fahlson, D. Jones, and D. Köhn, Active experiments stimulating waves and particle precipitation with small ionospheric barium releases, *J. Geophys. Res.*, 79, 2859-2867, 1974.
- Kelley, M. C., R. Pfaff, and G. Haerendel, Electric field measurements during the Condor critical velocity experiment, *J. Geophys. Res.*, 91, 9939-9946, 1986.
- Kelley, M. C., C. M. Swenson, N. Brenning, K. Baker, and R. Pfaff, Electric and magnetic field measurements inside a high-velocity neutral beam undergoing ionization, *J. Geophys. Res.*, 96, 9703-9718, 1991.
- Kintner, P. M., M. C. Kelley, G. Holmgren, and R. Boström, The observation and production of ion acoustic waves during the Trigger experiment, *J. Geophys. Res.*, 85, 5071-5077, 1980.
- Koons, H. C., and M. B. Pongratz, Ion cyclotron waves generated by an ionospheric barium injection, *J. Geophys. Res.*, 84, 533-536, 1979.
- Koons, H. C., and M. B. Pongratz, Electric fields and plasma waves resulting from a barium injection experiment, *J. Geophys. Res.*, 86, 1437-1446, 1981.
- Koons, H. C., J. L. Roeder, and W. B. Harbridge, Extremely low frequency wave analyzer, *J. Spacecr. Rockets*, 29, 606-607, 1992.
- Reasoner, D. L., Chemical-release mission of CRRES, *J. Spacecr. Rockets*, 29, 580-584, 1992.
- Swenson, C. M., M. C. Kelley, F. Primdahl, and K. D. Baker, CRIT II electric, magnetic, and density measurements within an ionizing neutral stream, *Geophys. Res. Lett.*, 17, 2337-2340, 1990.
- Whalen, B. A., et al., Waterhole auroral arc modification experiments: Electrodynamic response, *J. Geophys. Res.*, 90, 8377-8386, 1985.

H. C. Koons and J. L. Roeder, Space and Environment Technology Center, The Aerospace Corporation, P.O. Box 92957, Los Angeles, CA 90009. (e-mail: dirac2::koons;dirac2::roeder)

TECHNOLOGY OPERATIONS

The Aerospace Corporation functions as an "architect-engineer" for national security programs, specializing in advanced military space systems. The Corporation's Technology Operations supports the effective and timely development and operation of national security systems through scientific research and the application of advanced technology. Vital to the success of the Corporation is the technical staff's wide-ranging expertise and its ability to stay abreast of new technological developments and program support issues associated with rapidly evolving space systems. Contributing capabilities are provided by these individual Technology Centers:

Electronics Technology Center: Microelectronics, VLSI reliability, failure analysis, solid-state device physics, compound semiconductors, radiation effects, infrared and CCD detector devices, Micro-Electro-Mechanical Systems (MEMS), and data storage and display technologies; lasers and electro-optics, solid state laser design, micro-optics, optical communications, and fiber optic sensors; atomic frequency standards, applied laser spectroscopy, laser chemistry, atmospheric propagation and beam control, LIDAR/LADAR remote sensing; solar cell and array testing and evaluation, battery electrochemistry, battery testing and evaluation.

Mechanics and Materials Technology Center: Evaluation and characterization of new materials: metals, alloys, ceramics, polymers and composites; development and analysis of advanced materials processing and deposition techniques; nondestructive evaluation, component failure analysis and reliability; fracture mechanics and stress corrosion; analysis and evaluation of materials at cryogenic and elevated temperatures; launch vehicle fluid mechanics, heat transfer and flight dynamics; aerothermodynamics; chemical and electric propulsion; environmental chemistry; combustion processes; spacecraft structural mechanics, space environment effects on materials, hardening and vulnerability assessment; contamination, thermal and structural control; lubrication and surface phenomena; microengineering technology and microinstrument development.

Space and Environment Technology Center: Magnetospheric, auroral and cosmic ray physics, wave-particle interactions, magnetospheric plasma waves; atmospheric and ionospheric physics, density and composition of the upper atmosphere, remote sensing using atmospheric radiation; solar physics, infrared astronomy, infrared signature analysis; effects of solar activity, magnetic storms and nuclear explosions on the earth's atmosphere, ionosphere and magnetosphere; effects of electromagnetic and particulate radiations on space systems; space instrumentation; propellant chemistry, chemical dynamics, environmental chemistry, trace detection; atmospheric chemical reactions, atmospheric optics, light scattering, state-specific chemical reactions and radiative signatures of missile plumes, and sensor out-of-field-of-view rejection.